Appl. Phys. B 83, 51–54 (2006)
DOI: 10.1007/s00340-005-2051-7

Applied Physics B
Lasers and Optics

D. ALDERIGHI[1]
G. TOCI[1]
M. VANNINI[1]
D. PARISI[2]
S. BIGOTTA[2,✉]
M. TONELLI[2]

High efficiency UV solid state lasers based on Ce:$LiCaAlF_6$ crystals

[1] IFAC – CNR, Area della Ricerca edificio C, Via Madonna del Piano, 50019 Sesto Fiorentino (FI), Italy
[2] NEST – INFM, Dipartimento di Fisica, Universitá di Pisa, Largo Pontecorvo, 3, 56127 Pisa, Italy

Received: 27 May 2005/Revised version: 1 September 2005
Published online: 14 February 2006 •

ABSTRACT We report the spectroscopy and laser results of cerium-doped colquiriite $LiCaAlF_6$ (LiCAF) single crystals. High quality samples have been grown using the Czochralski technique and characterized by means of X-ray Laue diffractometry, absorption and emission spectra. Moreover, we measured the lifetime and deduced the emission cross-sections of the laser transition. Using this crystal we realized two lasers devices: a high-efficiency laser emitting at 289 nm with a repetition rate (RR) of up to 2 kHz and a widely tunable laser (from 280 nm to 317 nm) with an RR of up to 4.3 kHz. The high quality of the crystal made it possible to obtain the highest slope efficiency (49%) ever reported to our knowledge for a Ce:LiCAF laser.

PACS 42.55.Rz; 78.55.Hx; 81.10.Fq

1 Introduction

Laser sources emitting in the near ultraviolet (UV) spectrum are fundamental tools in a number of applications, such as the detection of atmospheric constituents and polluting gases (e.g. ozone, aromatic compounds, and SO_2), medical applications and fluorescence measurements. Excimer lasers, which are widely used in the medical field, have a scarce tunability and have several problems due to maintenance and ergonomic factors, such as the handling of aggressive gases and high voltages. Alternatively, tunable UV radiation is widely produced by harmonic generation from conventional solid state or dye-laser sources, in which the conversion process requires optimization of the system for each selected wavelength. Furthermore, losses of efficiency are present for each harmonic generation process. For these reasons, a solid state tunable laser with direct emission in the near UV is a very desirable breakthrough.

Cerium-activated colquiriite crystals have been indicated for more than a decade as a very promising active media suitable for such a device [1–6]. Among all the proposed hosts, the cerium-doped $LiCaAlF_6$ (Ce:LiCAF) is one of the most attractive because it shows the lowest attitude to color centers formation and excited state absorption that can hamper the laser action [7–9]. Furthermore, it exhibits wide tunability and high quantum efficiency. Many interesting laser results have been obtained with this material, as is reported in the literature: 60 mJ pulses have been obtained from a low RR, master oscillator power amplifier system [10], 530 mW average power delivered at 7 kHz RR in a dispersive cavity [11] and fs pulse amplification [12].

In the following section, we describe the growth process of the Ce:LiCAF crystal and its characterization. In the subsequent sections, we report on our laser devices obtained with this crystal.

2 Crystal growth and spectroscopic characterization

The samples under investigation are two $LiCaAlF_6$ single crystals doped with 1 at. % cerium. The crystal lattice of the colquiriite belongs to the D_{3d}^2 space group, with two formula units per unit cell and is derived from the Li_2ZrF_6 [13]. LiCAF crystals are trigonal with space group $P31C$, and lattice constants $a = 4.996$ Å and $c = 9.636$ Å.

The Ce^{3+} activator ion is 1.03 Å in ionic radius, and has a $4f^1$ electron configuration. The size of the Ce^{3+} suggests that the rare earth dopant would preferentially substitute into the Ca^{2+} sites (0.99 Å), rather than the Al^{3+} site (0.51 Å). The lithium site is not available for the substitution in both charge (+1 charge) and ionic radius (0.68 Å). Even though the divalent sites are large enough to accommodate the trivalent cerium ion, there is a charge imbalance which requires a compensation in the lattice in order to maintain charge neutrality. Charge compensation can be achieved by adding a monovalent cation such as Na^+ to a divalent site (Ca^{2+}) [14].

The crystal growth apparatus consists of a home-made Czochralski furnace with resistive heating. A vacuum treatment was carried out so as to eliminate water and oxygen from the growth chamber; the ultimate pressure was below 10^{-7} mbar. The crystals were grown using $LiCaAlF_6$ powder as the starting material, CeF_3 powder as the dopant, and NaF powder as the charge compensator. The concentration of Ce^{3+} and Na^+ in the starting material was 1 at. %. To avoid OH^- contamination, the powders were purified at AC Materials (Orlando, Fla. USA) at a high purity level (99.999%).

The growth process was carried out in a high purity Argon atmosphere (99.999%). The orientation of the crystals

✉ Fax: +39-0502214333, E-mail: bigotta@df.unipi.it

was controlled by using an *a*-axis oriented seed of undoped LiCAF. The diameter control of the boule was actuated by means of optical analysis, and the melt temperature was controlled by proportional integral derivative (PID). The pulling rate was 0.8 mm/h, the rotation rate was 12 rpm, and the temperature of the melt was 828.5 °C. At this temperature there is a considerable amount of lithium loss from the melt due to evaporation. This causes the melt to deviate from its initially stoichiometric condition. To avoid this effect, we added a concentration of 1 at. % of LiF to the starting materials. We grew two different boules of LiCAF single crystals, as shown in Fig. 1, with a diameter of 16 mm and a length of 80 mm.

The main difficulty that occurs during the growth of LiCAF is the formation of inclusions inside the crystal. This aspect is very important, since the inclusions seriously compromise the laser efficiency. In Fig. 1 we present two different boules pulled along the crystallographic *a*-axis. Boule a shows many inclusions distributed throughout all the crystal. During the first part of the growth, starting from the formation of the neck up to the point at which the diameter reached its final value, the diameter increased with a rate of 0.44 mm/h for 50 hours in a non-regular way. In fact, as can be seen in Fig. 1, the neck of the boule presents three clear oscillations, as a consequence of fluctuations of about 2 °C around the set temperature. On the contrary, sample b shows a very good diameter control, and the shape of the boule does not present any oscillation. During this growth, we reduced the diameter increase rate to a value of 0.33 mm/h for about 70 hours. In this case, the temperature fluctuations around the set point were greatly reduced (about 0.5 °C), and did not produce significant changes in the diameter. The first part of this boule has an high optical laser quality, as shown here as follows. Some inclusions are present only in the ending part of the boule.

From these results we deduced that the quality inside the boule is critically related to the variations in the crystal diameter and, consequently, to the temperature oscillations of the melt.

The single crystalline character of the sample was checked using a X-ray Laue technique that allowed us to identify the *a* and *c* crystallographic axes. For the laser experiment, the sample was cut at the Brewster angle with respect to the incident radiation and with the *c*-axis tilted by 36° relative to the

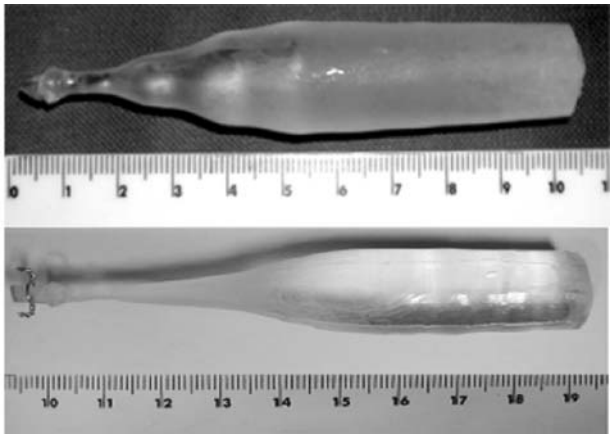

FIGURE 1 As-grown Ce-doped LiCAF single crystals pulled along the *a*-axis

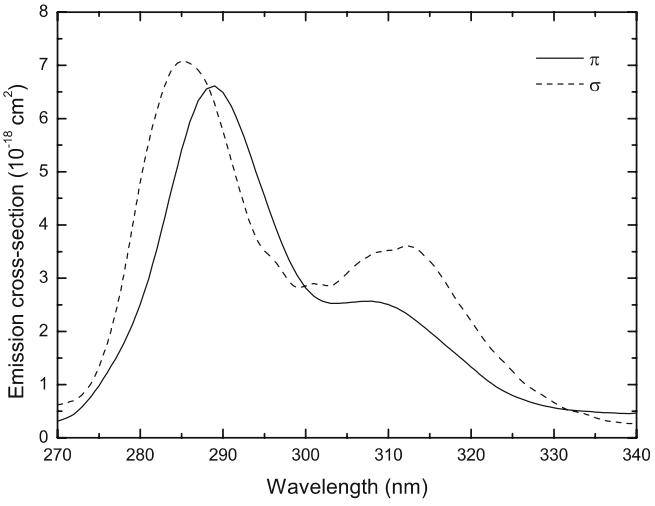

FIGURE 2 Polarized room temperature emission cross-sections of the 1% Ce:LiCAF crystal obtained from the emission spectra

polished faces. In this way, the electric field inside the active medium was parallel to the *c*-axis. The faces were polished to a high optical quality.

The samples have been characterized by means of absorption and emission spectra, performed for light polarized parallel (π) and perpendicular (σ) to the optical axis *c*. The maximum absorption is 3.7 cm^{-1} for both polarizations. On the basis of the luminescence data and the measured decay time ($\tau = 27.0 \pm 0.2$ ns), we evaluated the effective stimulated emission cross-sections by using the so-called β–τ method [16]. Figure 2 shows the emission spectra obtained with our experimental conditions. These spectra present two broad bands centred at 285.5 and 309.5 nm for the σ polarization, and at 288.7 and 308.2 nm for the π polarization. The peak emission cross-sections were 7.1×10^{-18} cm^{-2} at 285.5 nm and 6.6×10^{-18} cm^{-2} at 288.7 nm for the σ and the π polarization, respectively. All the spectroscopic data measured are in good agreement with the values reported in the literature [3].

3 Laser results

3.1 *High efficiency non-dispersive laser*

In this section we present the lasing action of the Ce:LICAF crystal in a non-dispersive cavity with longitudinal pumping at repetition frequencies from 100 Hz to 2 kHz. The pump source is an intra-cavity quadrupled (at 263.3 nm), Q-switched, lamp-pumped Nd:YLF laser, which delivers a maximum average power of 700 mW at 1 kHz RR.

In order to investigate the achievable performances by the newly grown crystals, the cavity and the pumping scheme were designed to obtain the highest slope and energy extraction efficiency (see Fig. 3). The resonator has an optical length of $l_c = 6.7$ cm and it consists of a high reflector (HR) mirror, with radius of curvature (ROC) 20 cm and transmission $T_p = 72\%$ at the pump wavelength, and of an output coupler (OC) mirror, ROC = 25 cm and reflectance $R = 60\%$ at the emission wavelength. The Brewster-cut Ce:LICAF crystal ($2 \times 3.3 \times 6.3$ mm^3) is kept at room temperature without heat sink. The pump beam is focused by a 10 cm focal length

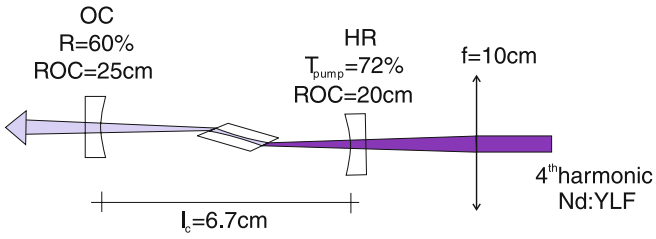

FIGURE 3 Scheme of the non-dispersive resonator for the high-efficiency longitudinally-pumped Ce:LICAF laser

fused silica lens. The pump waist radius is $w_p \simeq 95\,\mu$m, while the calculated mode waist in the Gaussian approximation is $w_0 = 85\,\mu$m; the corresponding maximum pump fluence is $F_p \simeq 2.6\,\mathrm{J/cm^2}$ with a pulse energy of 1.0 mJ delivered at 100 Hz. In this excitation condition the sample absorbs 68% of the pump energy corresponding to an effective absorption coefficient $\alpha = 1.8\,\mathrm{cm^{-1}}$. This value is slightly lower than the low intensity value ($\alpha_0 = 2.0\,\mathrm{cm^{-1}}$) at the same wavelength and this indicates that absorption in the crystal is slightly saturated. As a result, the pump energy is more uniformly transferred to the pumped volume, thus resulting in a better distribution of the population inversion along the longitudinal direction of the crystal.

In Fig. 4 the slope efficiency curves of this laser are shown for several RR up to 2 kHz, with respect to the absorbed pump energy. The pump energy was continuously varied by means of a $\lambda/2$ waveplate and a quartz cube polarizer. Near the threshold, a deviation from the linear behavior can be observed, which is due to the smaller fraction of the pump pulse exceeding the threshold power. The linear fit of the experimental data at 100 Hz RR (solid boxes) shows an energy slope efficiency $\eta_{sl} = 49\%$ with a threshold energy $E_{th} = 67\,\mu$J. To our knowledge, this is the highest slope efficiency value ever reported for a Ce:LICAF laser [17, 18] and this is an indication of the high quality of the crystal. It is worth noting that absorbed fraction of the pump energy is calculated using the value of the crystal absorption obtained at the maximum incident pump energy. As this value corresponds to a slightly saturated absorption, the values obtained for η_{sl} and the threshold energy are thus slightly underestimated with respect to the real values.

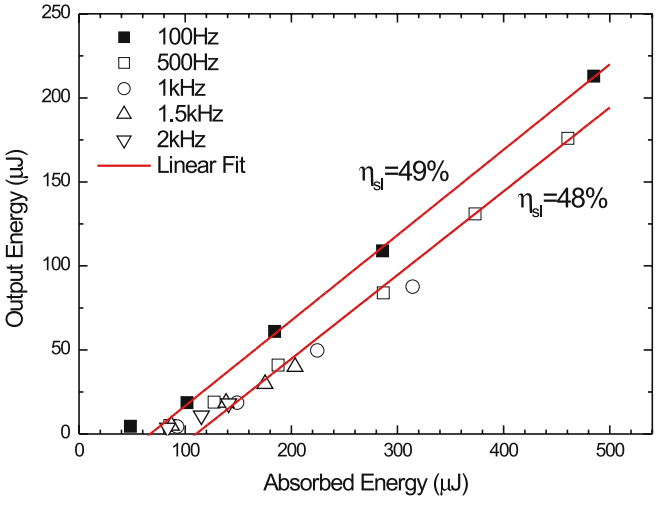

FIGURE 4 Efficiency curves at 100 Hz RR (*solid boxes*) and 500 Hz to 2 kHz RR (*open symbols*). *Lines* are linear fit of the experimental data

The slope efficiency in the same configuration for RR up to 2 kHz is reported again in Fig. 4 (open symbols). In comparison with the results obtained at 100 Hz, the fitted slope efficiency is slightly smaller (from 49% to 48%) and the threshold energy E_{th} increases up to 110 μJ. This behavior is probably due to the change of the pump pulse temporal profile for increasing RR. When the pulse RR is increased from 100 Hz to 2 kHz, the pump pulse duration (FWHM) lengthens from 100 ns up to 120 ns, and its rise time (from 10% to 90% of the peak) also increases from 35 to 50 ns, so that for a given pulse energy, the peak power is correspondingly reduced. These modifications of the pump pulse (which are more important when going from 100 Hz to 500 Hz) affect the overall efficiency of the Ce:LICAF laser in two ways: due to the short upper level lifetime, the increase in the rise time of the pump pulse determines a larger energy loss due to the spontaneous emission; furthermore, due to the lower peak power, an increasing fraction of the pump pulse on its trailing edge remains below threshold. These two effects determine the observed increase in the threshold energy and the small decrease in the slope efficiency.

On the other hand, the thermal load on the crystal seems to play a minor role in this regime of average pump power. This can also be seen from the graph of Fig. 4, where it appears that, for a given pump pulse energy, the output energy remains almost constant for a value of RR above 500 Hz despite the fact that the average absorbed power increases of a factor up to 4 across the explored RR range.

3.2 *Multi*-kHz *tunable laser*

To make the Ce:LICAF tunable source, we used the cavity scheme shown in Fig. 5, where we employed an intracavity Brewster-Brewster fused silica prism (indicated by P1) as a dispersive element.

The cavity mirrors are the HR (ROC = 20 cm) and the OC with $R = 75\%$ and ROC = 25 cm. The single pass optical length of the resonator is $l_c = 12.5$ cm and the Brewster-cut crystal, already described in the previous section, is centered with the waist pump mode in the middle. The calculated mode waist radius is $w_0 = 95\,\mu$m, which matches the pump spot radius. In this cavity configuration, we used a quasi-longitudinal

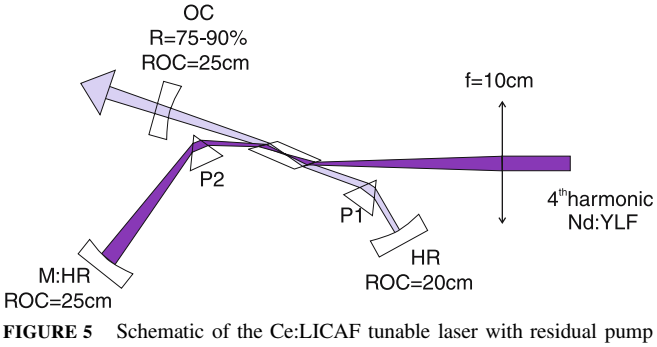

FIGURE 5 Schematic of the Ce:LICAF tunable laser with residual pump re-injection. *Light-coloured beam* is the laser beam, *dark beam* is the pump beam. The drawing is not in scale

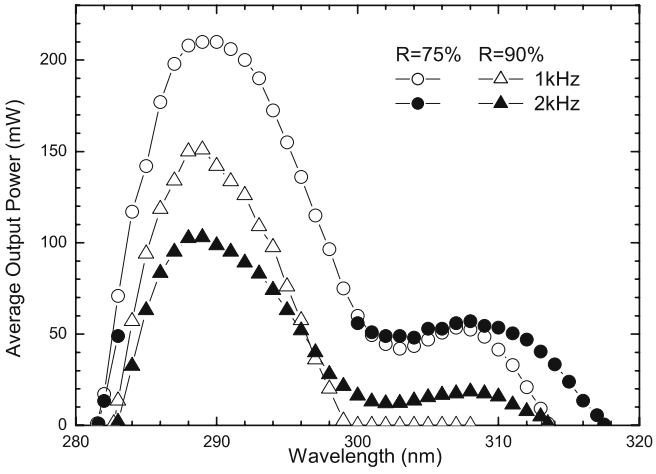

FIGURE 6 Tuning curves at RR = 1 kHz (*squares*) and 2 kHz (*triangles*) for two different OC: (*open symbols*) $R = 75\%$, ROC = 25 cm and (*full symbols*) $R = 90\%$, flat

pumping scheme with a small angle (less than 1 degree) between the pump beam and the laser mode. The pump energy transmitted by the crystal is also exploited, as the residual pump beam is extracted by means of the P2 prism and focused back into the crystal by the mirror M (ROC = 25 cm).

With respect to the linear cavity shown before, the higher l_c value due to the insertion of prisms P1 and P2 slightly reduces the overall efficiency of the laser; furthermore, the longer round trip time $2l_c/c \simeq 0.83$ ns increases the laser pulse build-up time with a correspondingly increased energy loss due to spontaneous emission during the first part of the pump pulse.

On the other hand, the detrimental effects caused by the cavity lengthening and by the reduction of the overlap between the pump and the laser mode volumes, due to the quasi-collinear pump scheme, are largely compensated by the direct injection of the pump beam (which allows to avoid the high loss caused by the pump injection through the end mirror) and by the use of the double pass pumping scheme. In fact, with the prism insertion and the double pass absorption, the pump pulse energy absorbed by the crystal is approximately $E_{abs} = [2A - A^2]E_p$, where E_p is the pump pulse energy available after the focusing lens, A is the single pass absorption in the crystal and we have neglected the losses on the prism and on the crystal surfaces. With $A \simeq 68\%$, this gives $E_{abs} = 0.90E_p$. On the other hand, in the longitudinal pumping configuration shown in Fig. 3 the energy absorbed by the crystal was only $E_{abs} = AT_pE_p \simeq 0.49E_p$ (where T_p is the transmission of the cavity end mirror at the pump wavelength). Moreover, the spatial distribution of the pumped volume is improved, because it is made more uniform along the crystal length, and the forward and the backward pump beam alignments can be separately optimized so as to maximize the overlapping with the laser mode. The tuning curves obtained with this cavity configuration are shown in Fig. 6 for RR = 1 kHz and 2 kHz. The tuning range spans 36 nm between 280 nm and 317 nm and the form is consistent with the π emission cross-sections formerly shown. At 1 kHz, the maximum output average power is 210 mW at the gain band peak (289 nm), with the $R = 75\%$ OC (open symbols). Comparison with the $R = 90\%$ OC (full symbols) shows that the tuning range is extended up to 317.5 nm towards the longer wavelength. In the case of OC with $R = 90\%$, the output power around the peak of gain band cannot be measured at RR = 1 kHz, because the high intra-cavity circulating fluence would damage the mirrors. The spectral line widths which we obtained are $\Delta\lambda \simeq 0.38$ nm at 289 nm with the $R = 75\%$ OC and $\simeq 0.54$ nm at 300 nm with the $R = 90\%$ OC, independently of the RR. $\Delta\lambda$ slightly decreases towards the shorter wavelength due to the increasing dispersion of the fused silica prism.

4 Conclusion

We have reported the spectroscopic characterization of a high quality Ce:LICAF crystal grown by means of the Czochralski technique. We reported the upper level lifetime and the emission cross-sections. The crystal was employed for the realization of two laser systems: a UV high-efficiency and a widely tunable multi-kHz laser, both pumped with the fourth harmonic of a Q-switched Nd:YLF laser. The high efficiency system exhibits the highest slope efficiency ever obtained for a Ce:LICAF laser (49%). The tunable laser shows a wide tunability range (280 to 317 nm) that has been achieved in the multi-kHz operation regime.

ACKNOWLEDGEMENTS The authors wish to thank Mrs. Ilaria Grassini for preparation of the samples and Arlete Cassanho and Hans Jenssen for helpful discussions. This work has been realized within the framework of collaboration the program between the CNR and MIUR, (Law 449/97).

REFERENCES

1 M.A. Dubinskii, V.V. Semashko, A.K. Naumov, R.Y. Abdulsabirov, S.L. Korableva, J. Mod. Opt. **40**, 1 (1993)
2 J.F. Pinto, G.H. Rosenblatt, L. Esterowitz, V. Castillo, G.J. Quarles, Electron. Lett. **30**, 240 (1994)
3 C.D. Marshall, J.A. Speth, S.A. Payne, W.F. Krupke, G.J. Quarles, V. Castillo, B.H.T. Chai, J. Opt. Soc. Am. B **11**, 2054 (1994)
4 N. Kodama, M. Yamaga, B. Henderson, J. Appl. Phys. **84**, 5820 (1998)
5 Z. Liu, N. Sarukura, M.A. Dubinskii, R.Y. Abdulsabirov, S.L. Korableva, J. Nonl. Opt. Phys. Mater. **8**, 41 (1999)
6 N. Sarukura, M.A. Dubinskii, L. Zhenlin, V.V. Semashko, A.K. Naumov, S.L. Korableva, R.Y. Abdulsabirov, K. Edamatsu, Y. Suzuki, T. Itoh, IEEE J. Sel. Top. Quantum Electron. **1**, 792 (1995)
7 D.J. Ehrlich, P.F. Moulton, R.M. Osgood, Jr., Opt. Lett. **4**, 184 (1979)
8 D.J. Ehrlich, P.F. Moulton, R.M. Osgood, Jr., Opt. Lett. **5**, 339 (1980)
9 T. Kozeki, Y. Suzuki, M. Sakai, H. Ohtake, N. Sarukura, Z. Liu, K. Shimamura, K. Nakano, T. Fukuda, J. Cryst. Growth **229**, 501 (2001)
10 Z. Liu, S. Izumida, H. Ohtake, N. Sarukura, K. Shimamura, N. Mujilatu, S.L. Baldochi, T. Fukuda, Jpn. J. Appl. Phys. II **37**, L1318 (1998)
11 A.J.S. McGonigle, D.W. Coutts, C.E. Webb, Opt. Lett. **24**, 232 (1999)
12 Z. Liu, T. Kozeki, Y. Suzuki, N. Sarukura, K. Shimamura, T. Fukuda, M. Hirano, H. Hosono, Jpn. J. Appl. Phys. I **40**, 2308 (2001)
13 K.I. Schaffers, D.A. Keszler, Acta Crystallogr. **C47**, 18 (1991)
14 V.K. Castillo, G.J. Quarles, J. Cryst. Growth **174**, 337 (1997)
15 K. Shimamura, N. Mujilatu, K. Nakano, S.L. Baldochi, Z. Liu, H. Ohtake, N. Sarukura, T. Fukuda, J. Cryst. Growth **197**, 896 (1999)
16 B. Aull, H. Jenssen, IEEE J. Quantum Electron. **QE-18**, 925 (1982)
17 A.J. McGonigle, D.W. Coutts, Laser Focus World **39**, 127 (2003)
18 D.W. Coutts, A.J.S. McGonigle, IEEE J. Quantum Electron. **QE-40**, 1430 (2004)